

# Steps in the negative-differential-conductivity regime of a superconductor

Milind N. Kunchur <sup>†\*</sup>, B. I. Ivlev <sup>†‡</sup>, and J. M. Knight <sup>†</sup>

<sup>†</sup>*Department of Physics and Astronomy  
University of South Carolina, Columbia, SC 29208  
\*<http://www.cosm.sc.edu/kunchur>*

and

<sup>‡</sup>*Instituto de Física, Universidad Autónoma de San Luis Potosí  
San Luis Potosí, S. L. P. 78000 Mexico*

Current-voltage characteristics were measured in the mixed state of  $\text{Y}_1\text{Ba}_2\text{Cu}_3\text{O}_{7-\delta}$  superconducting films in the regime where flux flow becomes unstable and the differential conductivity  $dj/dE$  becomes negative. Under conditions where its negative slope is steep, the  $j(E)$  curve develops a pronounced staircase like pattern. We attribute the steps in  $j(E)$  to the formation of a dynamical phase consisting of the successive nucleation of quantized distortions in the local vortex velocity and flux distribution within the moving flux matter.

In a type II superconductor, a magnetic field  $H$  above the lower critical value  $H_{c1}$  introduces flux vortices containing an elementary quantum of flux  $\Phi_o = h/2e$ , and interactions between the vortices tend to align them into a uniform lattice [1]. Extrinsic forces due to impurity pinning, thermal fluctuations, or dynamic melting can result in a disordered solid or liquid state instead of a crystalline lattice [2]; however, long-range repulsions between the vortices will still enforce a relatively uniform density. The system under study consists of a superconducting film in a perpendicular applied flux density  $B_o$  along  $\hat{z}$ , with a transport electric current density  $j$  and electric field  $E$  along  $\hat{y}$  in the plane of the film. The transverse component of  $E$  is negligible for this discussion and the vortices move with velocity  $v_\phi$  predominantly along  $\hat{x}$ .

A transport current exerts a Lorentz driving force  $\mathbf{F}_L = \mathbf{j} \times \Phi_o$  on the vortices and the motion is opposed by a viscous drag  $\mathbf{F}_d = -\eta \mathbf{v}_\phi$ , where  $\eta$  is the coefficient of viscosity. If we assume that pinning forces  $\mathbf{F}_p$  are negligible (because  $F_L \gg F_p$ ) then the steady state motion reflects a balance between driving ( $F_L$ ), drag ( $F_d$ ), and elastic forces ( $F_e$ ) on each vortex. For a perfectly uniform distribution, the net elastic force on each vortex vanishes resulting in free flux flow [3]. Then  $j\Phi_o = \eta v_\phi$  producing an Ohmic response approximated by [2,4]:  $\rho_f/\rho_n \approx B/H_{c2}(T)$ .

A different scenario prevails at ultra high dissipation levels and electric fields sufficient to alter the electronic distribution function and/or the electronic temperature. Here  $j(E)$  becomes non-linear and can develop an unstable region with negative differential conductivity (NDC) (region “C” in Fig. 1). Such unstable behavior and

NDC has been predicted by Larkin and Ovchinnikov (LO) for the regime near  $T_c$  [5], and has been experimentally well established [6,7]. In the LO mechanism, a non-equilibrium electronic distribution function leads to shrinkage of the vortex core by removal of quasiparticles from its vicinity [5,6]. In the opposite regime of  $T \ll T_c$  we have observed a qualitatively different type of instability [8,9] that seems to result from a temperature differential between the electronic system and lattice while maintaining an equilibrium-like distribution function (because electron-electron scattering is more rapid than electron-phonon scattering at low  $T$ ). In our low-temperature instability the vortex expands rather than shrinks, and viscous drag is reduced because of a softening of gradients of the vortex profile rather than a removal of quasiparticles. The standard LO instability near  $T_c$  occurs at values  $j^*$  and  $v^* = E^*/B$  (see Fig. 1) that are  $B$  independent, whereas in our low-temperature instability  $j^*$  and  $v^*$  have a  $\sim 1/\sqrt{B}$  dependence. This plays an important role in the appearance of a staircase at low temperatures but not at the higher temperatures of the previously well studied LO phenomenon. Theoretical and experimental details of the low-temperature instability are discussed elsewhere [8,10].

Fig. 1 suggests a qualitative picture of how the drag component ( $\eta v$ ) of the  $j(E)$  response might vary with  $E$  over its entire range. After the first “hump” (regions A, B, and C) because of a reduction in  $\eta$  by the mechanisms mentioned above,  $j(E)$  will rise again when  $v_\phi$  reaches some limiting value such as  $v_\infty \sim \xi/\tau_\Delta$ , where  $\xi = 1.5$  nm is the coherence length and  $\tau_\Delta = \hbar/\Delta \approx 4.7 \times 10^{-14}$  s is the order-parameter relaxation time. If the vortex density is non-uniform, an additional elastic term appears in  $j$ , namely  $j = (\eta v - F_e)/\Phi_o$ . We shall refer to the  $j(E)$  curve of Fig. 1 as the *primitive* curve, which applies to a hypothetical ensemble of uniformly packed vortices moving with identical velocities; an actual  $j(E)$  will not follow this behavior since, upon encountering a negative slope, the flux matter will become unstable and undergo a phase transition, such that at any given time there exist multiple vortex velocities (resulting in a composite response) and a non-uniform vortex density (resulting in elastic corrections). In effect some vortices will be travelling on the second positive slope “E” of Fig. 1 with  $v_\phi \sim v_\infty$  (in regions with reduced vortex density) and the rest will be travelling at a reduced velocity  $v_1 < v^*$  resulting in restabilization. Below we calculate the expected

composite response for one particular flux structure and show that it leads to a staircase in a natural way in rough agreement with the data.

The samples are *c*-axis oriented epitaxial films of  $\text{Y}_1\text{Ba}_2\text{Cu}_3\text{O}_{7-\delta}$  on (100)  $\text{LaAlO}_3$  substrates with  $T_c$ 's around 90K and of thickness  $t \approx 90$  nm. Electron-beam and optical-projection lithographies, together with wet etching in  $\sim 1\%$  phosphoric acid, were used to pattern bridges of widths  $w \approx 4\ \mu\text{m}$  and lengths  $l \approx 90\ \mu\text{m}$ . At the end of the lengthy fabrication, each microbridge is inspected by a variety of high-resolution optical probes for uniformity of width to ensure high reproducibility. Altogether ten samples were studied at 12 temperatures (1.6, 2.2, 6, 7, 8, 10, 20, 27, 35, 42, 50, 80 K) and at 11 flux densities (0.1, 0.2, 0.5, 1, 1.5, 2, 10, 11, 13, 13.5, 14 T). We always observe an instability with steps in the NDC region for all temperatures below  $T_c/2$  and for  $B$  values in the 1–14 T range. The electrical transport measurements were made with a pulsed constant voltage source, preamplifier circuitry, and a digital storage oscilloscope. The pulse rise times are about 100 ns with a duty cycle of about 1 ppm, resulting in effective thermal resistances of order  $1\ \text{nK}\cdot\text{cm}^3/\text{W}$ . The ability to hold the voltage constant across the sample allows investigation of the  $j(E)$  curve in the NDC region; however, once  $dj/dE$  becomes negative there will be a jump in the voltage until the chordal resistance of the sample has risen above the source impedance of the voltage source (including the resistance of the leads and contacts) allowing a stable steady state. Such forbidden gaps in  $E$  are visible in the last data plot at the onset of NDC. Each  $j(E)$  curve typically consists of 1000 separate points and each point requires averaging over several hundred pulses to obtain an adequate signal-to-noise ratio (SNR), so that a single curve takes several days to measure. Note that the  $j$  values in the experiment are an order of magnitude lower than the depairing current density [11]. Further details about the experimental techniques are discussed elsewhere [10,12].

Fig. 2 shows some examples of measured staircase patterns in the NDC regime. We found such patterns to be ubiquitous under most conditions of  $B_o$  and  $T$  (not close to  $T_c$ ). Fig. 2(a) shows the behavior at 11T and 27K. The main step features are seen to be reproducible between curves measured a week apart in opposite directions of changing  $E$ . Panel (b) shows 50-K 1-T  $j(E)$  curves for two different samples (sample X was measured 23 days after sample Z). Within the scatter and uncertainty in the absolute  $j$  values (due to uncertainty in the sample widths used to calculate  $j$  from  $I$ ), there appears to be some consistency in the main step features. The steepest NDC and most pronounced staircase patterns were observed at temperatures around one half of  $T_c$  and flux densities around 1 Tesla (where the intervortex separation  $a \simeq \sqrt{\Phi_o/B}$  becomes comparable to the penetration depth). Fig. 2(c) shows 50K curves for sample X at three  $B$  values over an extended range of  $E$ . The solid line fit

indicates linearity in  $1/E$  over the steep NDC portion. Other observed features are a convergence of curves in their NDC regions for different  $B_o$ 's (at fixed  $T$ ) and a growth in horizontal step size with increasing  $E$ .

Let us now consider the nature of the transition in the flux matter when the imposed electric field  $E_o$  exceeds  $E^*$  and enters the NDC region “C” of the primitive curve (Fig. 1). Since all the vortices could not be moving uniformly with  $v_\phi = E_o/B_o$  (for they would all be unstable) the flux matter must reorganize itself by the creation of moving defects in the regular vortex structure. The exact nature of the defects will depend on the vortex state. In a vortex solid there can be pairs of edge dislocations of different signs, or defect-interstitial pairs that conserve the total flux. If the moving vortex system is a liquid, the defect can be a finite magnetic spot or domain with a different flux density, since redistribution of a magnetic flux in a vortex liquid does not involve significant energy barriers [13]. In this Letter we present a simple calculation based on the magnetic domain approach, in order to provide a simple physical explanation of the effect. A detailed and more rigorous approach, which considers the distinction among the different possibilities listed above, will be presented elsewhere. In the reorganized flux structure some vortices at any given time will move on the second positive slope “E” with  $v_\phi \sim v_\infty$  while others move on the first slope “A” with  $v_1 < v^*$ , such that the composite macroscopic electric field across a sample length averages to  $E_o$ . The reorganized flux structure is influenced by several conditions: (1) The ends of the sample are at a fixed potential difference so the average electric field along any longitudinal path is close to the applied  $E_o$ ; (2) the current density integrated along any longitudinal path is approximately constant due to phase coherence (allowing for small variations in the vector potential); (3) the average flux density in the sample must equal the applied value  $B_o$ , otherwise the demagnetizing fields would diverge — this means that if defects are formed that have a suppressed local  $B$ , the flux density  $B_1$  in the outside bulk will increase to conserve the total flux so as to maintain  $\langle B \rangle = B_o$ ; (4) extended low  $B$  defects will tend to be stationary to reduce circulating electric fields around them, which would violate the first condition; (5) elastic forces between adjacent vortices — along with asymmetry in demagnetization (since  $l \gg w$ ) — will tend to discourage relative side-by-side motion and promote modulations in  $v_\phi$  and  $B$  that traverse the entire length of the sample; and (6) bulk elastic forces within the vortex matter will discourage continuous growth of defects but instead favour discontinuous nucleation of uniformly spaced defects of the smallest possible size ( $\sim 1$  lattice constant).

Considering the above guidelines, we estimate below the composite  $j(E)$  response for one simplified static scenario of the defect structure. We would like to emphasize that this is not presented as a comprehensive or unique solution to the vortex reorganization problem, but only used to provide a simple physical explanation

of the observed staircase behavior. Referring to Fig. 1, let the applied electric field just exceed the peak value  $E^*$ . The functional form of the primitive  $j(E)$  curve in the peak region is given by [8,10]  $j \sim (\sigma_n H_{c2}/B)E/[1 + (E/E^*)^2]$  with  $E^* = \sqrt{2\rho_n B n \Delta / (H_{c2} \tau_\epsilon)}$  and  $j^* = \sqrt{n \Delta H_{c2} / (2\rho_n B \tau_\epsilon)}$ . Some vortices are forced to move at higher velocity in order to restore stability. For the purpose of obtaining a rough estimate, let's assume that vortices move at  $v_\infty$  when they cross a longitudinal channel with reduced local  $B$  and enlarged flux lattice spacing  $A$  (The actual structure may consist of an array of smaller entities that nucleate at the sample edges and migrate inward.) The smallest width of this channel, consistent with continuity of flux and constancy of longitudinal  $E$ , is a single lattice spacing  $A = a(v_\infty/v_1)$ , where  $a$  and  $v_1$  are the lattice spacing and velocity of the “bulk” vortex matter outside the channels. As soon as the first defect is nucleated, the flux density  $B_1$  in the bulk increases discontinuously<sup>1</sup> from  $B_o$  to  $B_o w / (w - A)$  and  $v_1$  drops from  $E_o/B_o$  to  $E_o(w - A)/(B_o w)$ . This immediately stabilizes flux flow in the bulk since  $E^* \propto \sqrt{B}$  increases and these vortices drop back on the positive slope “A” (in Fig. 1). As the applied  $E_o$  is increased further nothing more happens until  $v_1$  reaches the new peak value  $E^*/B_1$ . Then a second defect is nucleated and the process keeps repeating itself until the defects fill about half the sample area, at which point it becomes energetically favourable to continuously expand existing defects. The top of each step corresponds to  $j = j^*(B_1)$  for each new  $B_1$ . Since  $j^* \propto 1/\sqrt{B}$  and  $E^* \propto \sqrt{B}$ , the staircase shows an overall downward trend with  $j \sim 1/E$  dependence that does not depend on  $B_o$  (causing curves with different applied  $B_o$  to converge). Both of these behaviors can be seen in Fig. 2(c). Fig. 3 shows experimental and numerically computed  $j(E)$  curves at  $T=50\text{K}$  and  $B=1, 1.5$ , and 2 Tesla. The two sets of curves show similar qualitative trends and have roughly comparable magnitudes. Note: The curves computed from the model have no adjustable parameters — the values for  $1/\sigma_n \simeq \rho_n = 57\mu\Omega\text{-cm}$  and  $H_{c2} = 120\text{ T}$  come from the literature [10,14] and  $E^* = 35\text{ V/cm}$  (at one value of  $B = 1.5\text{ T}$ ) is taken from the measurement.

To summarize, we have investigated the transport response of a superconductor into the regime of negative differential conductivity beyond the low-temperature instability. A qualitatively new behavior was observed in the form of steps in the  $j(E)$  curve. The observed behavior is consistent with the restabilization of a moving vortex distribution by the formation of a dynamical phase with distortions in the local flux density and vortex velocity. While we do not undertake a detailed theoretical

investigation of the exact nature of the dynamical phase, we hope our experimental results will stimulate such further work. Recently other interesting but separate effects have been seen in the highly driven vortex state by the Huebener group, which include time dependent oscillations and hysteretic steps resulting from tunneling between neighbouring vortices [15]. The steps in our effect are time-independent and non-hysteretic, and are analogous to the Gunn effect in semiconductors, where electric-charge modulations lead to steps in  $j(E)$  in the NDC regime.

The authors acknowledge useful discussions and other assistance from D. K. Christen, J. M. Phillips, M. Geller, A. Koshelev, R. P. Huebener, N. Schopohl, J. Blatter, and V. Geshkenbein. This work was supported by the U. S. Department of Energy through grant number DE-FG02-99ER45763.

- 
- [1] A. A. Abrikosov, Zh. Eksp. Teor. Fiz. **32**, 1442 (1957) [Sov. Phys. JETP **5**, 1174 (1957)].
  - [2] J. Blatter *et al.*, Rev. Mod. Phys. **66**, 1125 (1994), and references therein.
  - [3] M. N. Kunchur, D. K. Christen, and J. M. Phillips, Phys. Rev. Lett. **70**, 998 (1993).
  - [4] J. Bardeen and M. J. Stephen, Phys. Rev. **140**, A1197 (1965); and A. I. Larkin and Yu. N. Ovchinnikov, in *Nonequilibrium Superconductivity*, D. N. Langenberg and A. I. Larkin, eds. (Elsevier, Amsterdam, 1986), Ch. 11.
  - [5] A. I. Larkin and Yu. N. Ovchinnikov, Zh. Eksp. Teor. Fiz. **68**, 1915 (1975) [Sov. Phys. JETP **41**, 960 (1976)].
  - [6] W. Klein, R. P. Huebener, S. Gauss, and J. Parisi, J. Low Temp. Phys. **61**, 413 (1985).
  - [7] L. E. Musienko, I. M. Dmitrenko, and V. G. Volotskaya, Pis'ma Zh. Eksp. Teor. Fiz. **31**, 603 (1980) [JETP Lett. **31**, 567 (1980)]; S. G. Doettinger *et al.*, Phys. Rev. Lett. **73**, 1691 (1994); A. V. Samoilov *et al.*, Phys. Rev. Lett. **75**, 4118 (1995); Z. L. Xiao *et al.*, Phys. Rev. B **53**, 15265 (1996) and S. G. Doettinger and R. P. Huebener, Chin. J. Phys. **34**, 527 (1996).
  - [8] M. N. Kunchur, to be published.
  - [9] M. N. Kunchur, B. I. Ivlev, and J. M. Knight, Bull. Am. Phys. Soc. **46**, 517 (2001).
  - [10] M. N. Kunchur *et al.*, Phys. Rev. Lett. **84**, 5204 (2000).
  - [11] M. N. Kunchur, D. K. Christen, C. E. Klabunde, and J. M. Phillips, Phys. Rev. Lett. **72**, 752 (1994).
  - [12] M. N. Kunchur, Mod. Phys. Lett. B. **9**, 399 (1995).
  - [13] S. Chakravarty, B. I. Ivlev, and Yu. N. Ovchinnikov, Phys. Rev. Lett. **64**, 3187, (1990).
  - [14] H. Nakagawa, N. Miura, and Y. Enomoto, J. Phys.: Condens. Matter **10**, 11571 (1998) and references therein; and U. Welp *et al.*, Phys. Rev. Lett. **62**, 1908 (1989).
  - [15] A. Wehner, O. M. Stoll, R. P. Huebener, and M. Naito, Phys. Rev. B **63**, 144511 (2001); O. M. Stoll *et al.*, Phys. Rev. Lett. **81**, 2994 (1998); and S. G. Doettinger, R. P.

---

<sup>1</sup>These estimates neglect the relatively small flux ( $B_1 A l v_1 v_\infty$ ) through the defects, which, however, is included in the numerically calculated curves of Fig. 3(b).

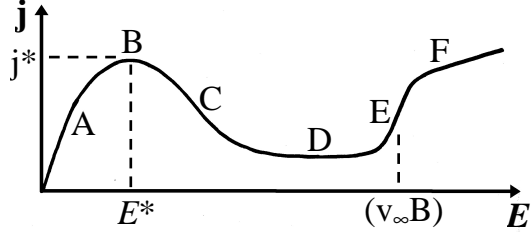


FIG. 1. Schematic diagram for a primitive  $j(E)$  curve for moving flux vortices distributed with uniform density and moving with the same velocity. The net elastic force  $F_e$  on each vortex vanishes and the Lorentz driving force  $F_L$  is balanced by the viscous drag  $F_d$  so that  $j = \eta v / \Phi_o$ . Experimentally only the regime “A” is accessible. Beyond the peak at “B”, unstable dynamics destroys the perfect spatial homogeneity of the vortex distribution and leads to non-vanishing elastic forces so that  $j = (\eta v - F_e) / \Phi_o$ . Now vortices travel in differing elastic environments and at unequal velocities such that each vortex is traveling on either positive slope “A” or “E” on the primitive  $j(E)$  curve appropriate to its local instantaneous environment. The positive slope “E” arises upon reaching some limiting velocity  $v_\infty < \xi / \tau_\Delta$  and “F” is entered when the sample is driven normal.

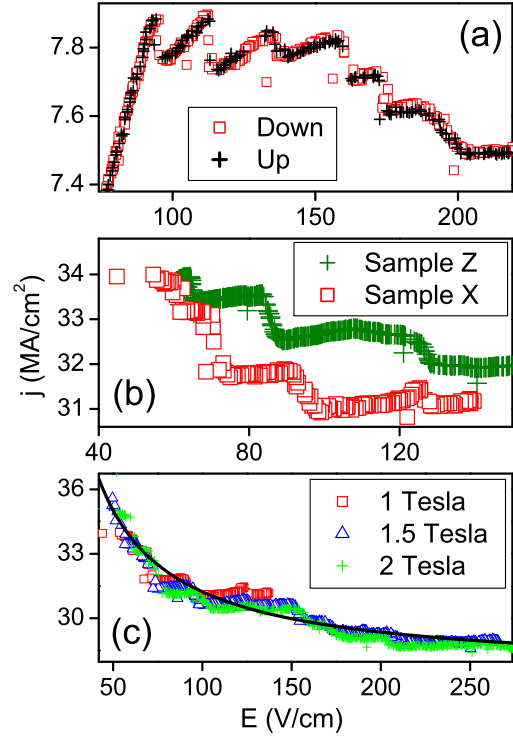


FIG. 2. (a) Experimental  $j(E)$  curves for sample X at  $B_o=11\text{T}$  and  $T=27\text{ K}$ . The two curve sets were measured in increasing (up) and decreasing (down)  $E$  to confirm reproducibility and absence of hysteresis. (b) Magnified view of experimental  $j(E)$  curves for two different samples at 50 K and 1 T (sample X was measured 23 days after sample Z). The step features show some consistency within the scatter of the data and uncertainties in the two sample widths used to calculate  $j$ . (c) 50K low- $B$   $j(E)$  curves for sample X over an extended  $E$  range showing overall linearity in  $1/E$ ; the solid line represents  $j = 27 + 375/E$ .

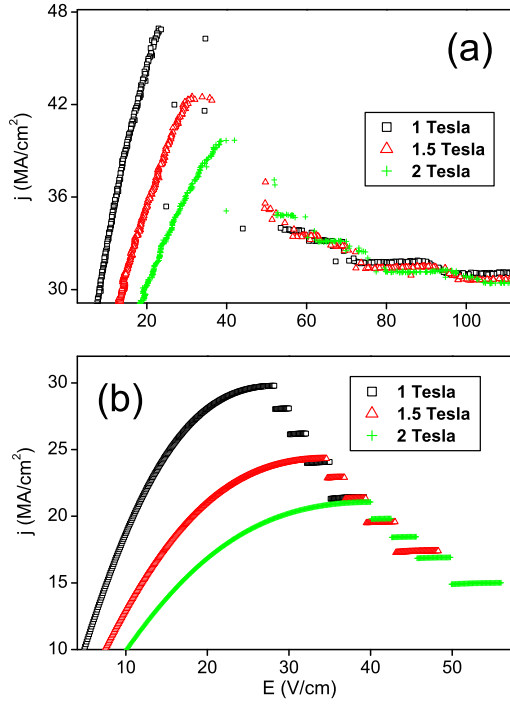


FIG. 3. (a) Experimental  $j(E)$  curves for sample X at  $T=50$  K and  $B=1, 1.5$ , and 2 T. In their NDC regimes, the curves collapse onto an approximately common behavior, where  $j$  is roughly linear in  $1/E$ . There are forbidden gaps in  $E$  just beyond the peak, when the sample's resistance is less than the voltage source impedance, as discussed in the text. (b) Theoretical  $j(E)$  curves for the same  $T$  and  $B$ 's, calculated from the simple model based on dynamical flux reorganization (the model has no fitting parameters).